In-Situ Polarization-Dependent Total-Reflection Fluorescence XAFS Studies on the Structure Transformation of Pt Clusters on α-Al_2O_3(0001)

Kiyotaka Asakura,[†] Wang-Jae Chun,[‡] Masayuki Shirai,[‡,§] Keiichi Tomishige,[‡,||] and Yasuhiro Iwasawa*,[||]

Research Center for Spectrochemistry, Faculty of Science, The University of Tokyo, Hongo, Bunkyo-ku, Tokyo 113, Japan, Department of Chemistry, Graduate School of Science, The University of Tokyo, Hongo, Bunkyo-ku, Tokyo 113, Japan, Institute for Chemical Reaction Science, Tohoku University, Katahira, Sendai 980-77, Japan, and Department of Applied Chemistry, Graduate School of Engineering, The University of Tokyo, Hongo, Bunkyo-ku, Tokyo 113, Japan

Received: January 31, 1997; In Final Form: April 18, 1997[⊗]

Structures of Pt species derived from $Pt_4(\mu\text{-}CH_3COO)_8$ on an α-Al_2O_3(0001) single-crystal surface were studied by means of in-situ polarization-dependent total reflection fluorescence XAFS (EXAFS and XANES) techniques. The Pt_4 cluster framework was destroyed upon the deposition of $Pt_4(\mu\text{-}CH_3COO)_8$ by the reaction on the α-Al_2O_3 surface at room temperature. The isolated Pt species were converted to one-atomic layer thick Pt rafts with the Pt−Pt distance of 0.273 nm when the cluster was treated with H_2 at 373 K. The raftlike Pt clusters were stabilized by the formation of direct Pt−O−Al bonding with the α-Al_2O_3 surface. The raftlike Pt clusters were redispersed to isolated oxidized Pt species by the reaction with NO. They were also transferred to three-dimensional Pt particles by reduction with H_2 at 773 K.

1. Introduction

Industrial metal catalysts are usually used as metal particles supported on high surface area metal oxide surfaces. The role of support oxides is not only to disperse the metal particles but also to modify the morphology, orientation, and electronic state of the metal particles through metal−support interaction, which are the most relevant factor to supported metal catalysis. EXAFS (extended X-ray absorption fine structure) is regarded as a powerful tool to gain the information about the morphology of metal particles and metal−support bonding. The particle morphology can be obtained by the analysis of the coordination number of metal−metal bonding.[1] The metal−support distance can be determined by detecting the EXAFS signal of atoms (mostly oxygen) at the support surface. However, it is not straightforward to obtain such a precise type of structural information from conventional EXAFS for powder catalyst sample because of the following reasons. First, the coordination number determined by EXAFS suffers from many factors like the effects of thermal and static disorder or asymmetry of pair distribution function.[2,3] Second, the metal−support bond, especially metal−oxygen bond with a small coordination number, has a small contribution to whole EXAFS spectra and is hindered by the metal−metal bond because the EXAFS oscillation for oxygen does not continue to the high k-region.

The amplitude of EXAFS oscillation depends on the direction of X-ray electric-field vector $\vec{\epsilon}$.[2,3] As a result the effective coordination number, N^* is expressed by eq 1:

$$N^* = 3\sum_j \cos^2\theta_j \qquad (1)$$

where θ_j is an angle between the polarization vector $\vec{\epsilon}$ and the bond vector $\vec{r}_j$. When the polarization vector is parallel to the surface (s-polarization), EXAFS will provide the information on the bondings parallel to the surface. When the polarization vector is perpendicular to the surface (p-polarization), the information about the structure perpendicular to the surface, i.e., the metal−support bond is selectively obtained.

Since the conventional supported metal catalysts are used in a powder form, the EXAFS oscillations are averaged over all directions. On the other hand, when the flat oxide substrates are used, the structural information parallel and perpendicular to the surface can be separately obtained by the polarization-dependent EXAFS measurements. However, a problem is to measure the surface species of low concentrations. Concentrations of monolayer metal on a flat surface are in the range 10^{14}−10^{15} atoms cm^{-2}, which is 4−5 orders of magnitude lower than concentrations of metals for conventional catalysts in a powder form. Usually fluorescence yield detection is more preferable for dilute samples than monitoring of direct absorption. In a soft X-ray region, the fluorescence-detection mode successfully gives the EXAFS signals with high quality[4−7] and the polarization-dependent EXAFS studies determine the adsorption sites of lighter elements such as C, O, S, Cl, and P.[8,9] On the other hand, most of the catalytically important elements have the X-ray absorption edges higher than 4 keV. The X-ray with such a high energy can penetrate deeply into the bulk, yielding a large amount of scattering X-rays which make it difficult to measure monolayer species supported on the flat substrate. When the X-ray hits on the flat substrate with the incident angle less than the critical angle δ_c, it undergoes a total reflection and penetrates only a few nanometers into the bulk. Consequently the scattering X-ray from the bulk is dramatically reduced.[10] After Heald et al. showed the possibility of the detection of EXAFS signals from a monolayer Au film deposited on a flat glass substrate by use of a total reflection fluorescence technique,[11] the total-reflection fluorescence EXAFS technique has been applied to semiconducting materials, electrodes, and corrosive surfaces.[12] We have applied this technique to catalytically interesting systems.[13−17] By analyzing the polarization dependence of EXAFS amplitude, we have revealed the orientation and growth mode of catalytic active species such as

---

[†] Research Center for Spectrochemistry.

[‡] Department of Chemistry.

[§] Institute for Chemical Reaction Science.

[||] Department of Applied Chemistry.

[⊗] Abstract published in *Advance ACS Abstracts,* June 15, 1997.

S1089-5647(97)00394-5 CCC: $14.00

SCHEME 1: Preparation Route of Pt Cluster on α-Al_2O_3(0001)

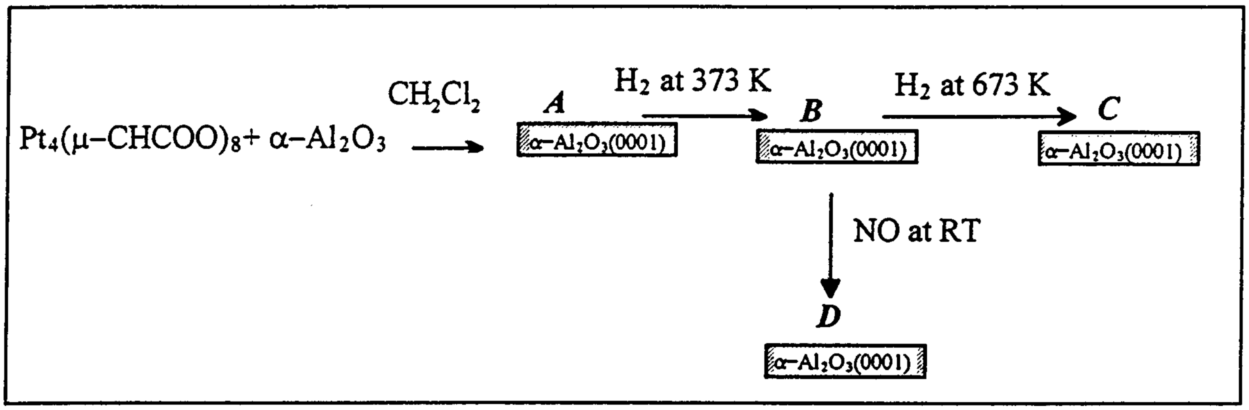

Co oxides and Cu oxides on flat inorganic oxide substrates as model systems for supported powder catalysts.

XANES (X-ray absorption near edge structure) spectra give information about electronic state and geometrical configuration and also show similar polarization dependence. Thus the combination of EXAFS and XANES, so-called XAFS (X-ray absorption fine structure), will give clear insight into the morphology, orientation, and metal−support interaction.

Moreover, the fluorescence XAFS allows us to carry out in-situ measurements on the structure of catalysts in the working conditions. We have constructed an in-situ chamber for polarization-dependent total-reflection fluorescence EXAFS measurement under various conditions from UHV (10^{-9} Pa) to high pressure (10^5 Pa) and from low temperature (100 K) to high temperature (800 K).[18] In this paper this in-situ chamber was employed for the measurement of the polarization-dependence total-reflection fluorescence XAFS (hereinafter we use abbreviation of PTRF-XAFS) for Pt species deposited on α-Al_2O_3(0001) using a $Pt_4(\mu\text{-}CH_3COO)_8$ complex as a precursor. The PTRF-XAFS technique demonstrated that isolated Pt monomeric species and one-atomic layer thick Pt rafts were formed on the α-Al_2O_3(0001) surface and reversibly transformed between them depending on the treatment and the atmosphere.

2. Experimental Section

2.1. Preparation of Materials. The cluster [$Pt_4(\mu\text{-}CH_3COO)_8$] was prepared following the literature.[19−21] An optical-grade polished α-Al_2O_3(0001) crystal was purchased from Earth Jewelry Co. The single crystal (10 × 30 × 1 mm^3) was calcined at 573 K for 2 h followed by evacuation at the same temperature for 1 h. The preparation steps are summarized in Scheme 1. Pt was deposited on the α-Al_2O_3(0001) surface by a dropwise impregnation method using a CH_2Cl_2 solution of [$Pt_4(\mu\text{-}CH_3COO)_8$] in the in-situ chamber[18] under a flow of high purity Ar (99.999%). The loading was estimated to be 1.5 Pt_4 nm^{-2} by XPS, which corresponds to an atomic ratio of platinum:surface oxygen = 4:10. The solvent was removed by evacuation under high vacuum at room temperature. The incipient supported sample **A** was then reduced at 373 K with H, (13.3 kPa) to form species **B** in the chamber. The species **B** was further reduced to species **C** by H_2 (13.3 kPa) at 673 K. Species **B** was also exposed to NO (1.33 kPa) at room temperature in the chamber (Species **D**).

2.2. PTRF-XAFS Measurements. The details of the in-situ XAFS chamber was described elsewhere.[18] Here we briefly describe the in-situ XAFS chamber, in which the XAFS spectra can be obtained under various conditions: from high vacuum (1 × 10^{-9} Pa) to high pressure (1 × 10^5 Pa) and from low temperature (100 K) to high temperature (800 K). A wide degree (100°) of rotation of the sample around the X-ray light axis enables us to measure the XAFS of the same sample in different X-ray polarization vectors without exposure to air. The fluorescence X-ray was detected by an NaI(Tl) scintillation counter which can be set close to the sample surface. The XAFS was measured at BL-7C of the Photon Factory in the National Laboratory for High Energy Physics (KEK-PF) using Si (111) sagittal focusing double-crystal monochromator.[22] Higher harmonics were removed by a double mirror made from fused quartz. The energy resolution was about 2 eV at 9 keV. The incident X-ray was monitored by a 5.5 cm ionization chamber filled with N_2 gas. Although it is better to measure Pt L_1-edge because eq 1 can be directly used for the analysis of the polarization dependence of EXAFS amplitude, the edge height of Pt L_1 was so small that the EXAFS oscillation tolerable for data analyses could not be obtained. Instead, we measured Pt L_3-edge spectra. Thus eq 1 should be modified as discussed later. All measurements were carried out at room temperature. One of the difficulty in the total-reflection fluorescence technique is diffraction from the single-crystal substrate. We can remove it by putting small pieces of lead plates at the positions of the detector window on which the Bragg diffractions hit. The other one is low intensity of the signals. The X-ray beam was collimated onto the substrate surface using a pinhole to eliminate undesirable scattering from the other part than substrate surface. It took 12 h to obtain a whole spectrum. The species A was measured under high-vacuum conditions. The measurements of samples B and C were done in the presence of H_2 and the measurement of sample D was performed under NO atmosphere.

2.3. Data Analysis. The EXAFS spectra were calculated directly from the ratio of the fluorescence from the sample to the incident X-ray signal detected by an ionization chamber (I_f/I_o) without any correction for self absorption because the Pt atoms were located only on the surface. The EXAFS oscillation $\chi(k)$ was extracted from the spectra by a cubic spline method and normalized by the edge height using EXAFS analysis program REX. The energy dependence of the edge height was taken into account using McMaster equation.[23] The origin of kinetic energy of photoelectron was temporarily taken in an inflection point of the edge jump. The Fourier filtered data were then analyzed by curve fitting analysis using eq 2:

$$\chi(k_j) = \sum_j \frac{N_j^* F_j(k_j)}{k r_j^2} \exp(-2\sigma_j^2 k_j^2) \exp(-2r_j/\lambda_j) \sin(2k_j r_j + \phi_j(k_j)) \quad (2)$$

where k_j, r_j, σ_j, λ_j, $F_j(k)$, and $\phi_j(k)$ are the wave-number of the photoelectron, the interatomic distance, the Debye−Waller factor, the mean free path of photoelectron, the backscattering amplitude function, and phase shift function for the jth shell, respectively. The $F_j(k)$ and $\phi_j(k)$ for Pt−Pt are derived from Pt foil. Those for Pt−O were calculated from feff v5.05 with Pt−O = 0.20 nm.[24] Since the absolute value of the theoretically derived amplitude is smaller by a factor of 0.7−0.9 than the actual amplitude, it was corrected by using the coordination number of 6 for Pt−O bonding in $(NH_4)_4[H_4PtMo_7O_{24}]$. The origin of photoelectron kinetic energy was adjusted using the following relation 3 in the curve-fitting process:

$$k_j^2 = k^2 - 2m\Delta E_j/\hbar \tag{3}$$

where ΔE_j and m are the deviation of the origin of photoelectron kinetic energy and the mass of electron, respectively.

Errors in curve-fitting analysis were estimated when ϵ_v^2 defined in eq 4 exceeds 1 according to the report of Committee on Standards and Criteria in X-ray Absorption Spectroscopy.[25]

$$\epsilon_\nu^2 = (N_{idp}/(N_{idp} - p))(1/N_{data})\sum[(\chi_{obs}(k) - \chi_{cal}(k))^2/\sigma_{error}^2] \tag{4}$$

where p is a number of the used fitting parameters; N_{data} is a number of data points; $\chi_{\mathrm{obs}}(k)$, $\chi_{\mathrm{cal}}(k)$ and σ_{error} are observed and calculated $\chi(k)$ and the estimated error, respectively. In this work we took into account only statistical errors. The fitting parameters are N_{idp} is a number of freedom calculated by[26]

$$N_{\mathrm{idp}} = 2\Delta k\Delta r/\pi + 2 \tag{5}$$

where Δk and Δr are the ranges of the Fourier transformation in r and k space. Normally p is 4(N,r,ΔE,$\Delta\sigma^2$) and N_{idp} is 6.6 for 1 shell fitting.

The eq 1 is no longer valid for L_3-edge spectra because the L_3-edge EXAFS corresponds to the transition of angular momentum from $l = 1$ to $l = 0$, 2. Therefore, the polarization dependence of EXAFS is expressed by eq 6 for $L_{2,3}$ edges,[27] instead of eq 1.

$$\chi(k) = \sum_j \frac{F_j(k)}{kr_j^2} \exp(-2\sigma_j^2 k^2) \exp(-2r_j/\lambda) \times \{{}^1/_2(1 + 3\cos^2\theta_j)|M_{21}|^2 \sin(2kr_j + \phi_{2j}) + {}^1/_2|M_{01}|^2 \sin(2kr_j + \phi_{0j}) + M_{01}M_{21}(1 - 3\cos^2\theta_j)\sin(2kr_j + \phi_{02j})\}/(|M_{21}|^2 + {}^1/_2|M_{01}|^2) \tag{6}$$

where M_{01} and M_{21} are dipole moments for the transitions from $l = 1$ to $l = 0$ and $l = 2$, respectively. ϕ_{0j}, ϕ_{2j}, and ϕ_{02j} are phase shift functions for the transitions from $l = 1$ to $l = 0$, from $l = 1$ to $l = 2$ and their cross term, respectively. Since (M_{01}/M_{21}) is about 0.2, we adopted the following assumptions for simplification in the present EXAFS analysis: (i) $\phi_{02j}(k) = \phi_{2j}(k)$, (ii) $(M_{01}/M_{21}) = 0.2$, (iii) $(M_{01}/M_{21})^2$ is negligible small. Then the eq 6 can be simplified to eq 7:[28]

$$\chi(k_j) = \sum_j N_j^* \frac{F_j(k)}{kr_j^2} \exp(-2\sigma_j^2 k_j^2) \exp(-2r_j/\lambda_j) \sin(2k_j r_j + \phi_{2j}(k_j)) \tag{7}$$

In this case N^* is expressed as follows:

$$N_j^* = \sum_k (0.7 + 0.9\cos^2\theta_k) \tag{8}$$

Note that the polarization dependence for L_3 edge is not perfect and one may observe Pt−X bonding even though the Pt−X bond direction is perpendicular to the X-ray polarization. In this paper we use the terms, s-polarization and p-polarization, which mean that the electric-field vectors are parallel to the surface and perpendicular to the surface, respectively.

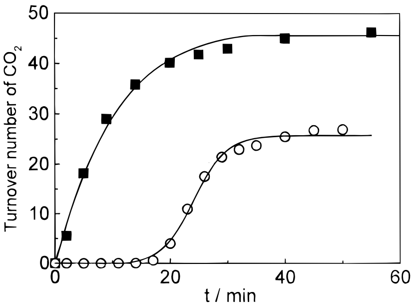

Figure 1. The turnover number of formed CO_2 per Pt_4 cluster during HCOOH decomposition reaction on the Pt species derived from $Pt_4(\mu\text{-}CH_3COO)_8/\alpha\text{-}Al_2O_3$ (■) and $Pt_4(\mu\text{-}CH_3COO)_8/SiO_2$ (○) at 288 K.

2.4. Catalytic Reaction. Catalytic activity for decomposition reaction of HCOOH on the α-Al_2O_3-supported $Pt_4(\mu\text{-}CH_3COO)_8$ powder was checked in a closed circulating system connected to a gas chromatography (Shimadzu Co, GC-8A) with a Poracpack PS column. The pressure of HCOOH was 1.47 kPa and the reaction temperature was 288 K.

3. Results

3.1. Catalytic Performance. Figure 1 shows the activity of $Pt_4(\mu\text{-}CH_3COO)_8$ dispersed on α-Al_2O_3 for the HCOOH decomposition reaction at 288 K. HCOOH was selectively decomposed to CO_2 and H_2 without any formation of CO and H_2O, contrasted to the HCOOH decomposition on Al_2O_3-supported Pt particles prepared by a traditional impregnation method using an aqueous solution, followed by the reduction with H_2 where both $CO_2 + H_2$ and $CO + H_2O$ were produced with a much lower activity. For comparison, the activity of $Pt_4(\mu\text{-}CH_3COO)_8$ supported on SiO_2 is shown in Figure 1.[29] As has already been reported, the SiO_2-supported $Pt_4(\mu\text{-}CH_3COO)_8$ showed a long induction period which became much longer than that for DCOOH and DCOOD.[29] The reaction on the SiO_2-supported $Pt_4(\mu\text{-}CH_3COO)_8$ terminated at ca. 10 min after the reaction initiation because the Pt species was reduced to Pt metal particles during the reaction. Unlike the SiO_2-supported Pt species, Pt species on α-Al_2O_3 did not show any induction period. The initial rate for the formation of CO_2 per Pt_4 (turnover frequency) was 4.4 min^{-1} which is twice as large as the maximum reaction rate for the $Pt_4(\mu\text{-}CH_3COO)_8/SiO_2$.

3.2. A Structure of Pt Species A. Figure 2A shows the EXAFS oscillations parallel (s-polarization) and perpendicular (p-polarization) to the α-Al_2O_3(0001) surface. The period and amplitude of the EXAFS oscillations in both directions are similar with each other. The corresponding Fourier transforms over k = 30−90 nm^{-1} give one peak around 0.17 nm (phase shift: uncorrected) for both directions as shown in Figure 2B. The original cluster $Pt_4(\mu\text{-}CH_3COO)_8$ has the Pt−Pt distance at 0.2495 nm which will give the Fourier transform peak around 0.20 nm (phase shift: uncorrected).[29] However, there was no peak in this region for both s and p-polarizations, indicating that the Pt4 cluster framework was destroyed. Moreover, no peak corresponding to Pt−Pt bond of Pt metal particles was observed around 0.25 nm (phase shift: uncorrected) in the Fourier transforms for both directions. Thus Pt atoms are monoatomically dispersed on the α-Al_2O_3 surface by the interaction with the substrate surface.

We carried out the curve fitting analysis on the inversely Fourier transformed data of the first peaks filtered over 0.1−

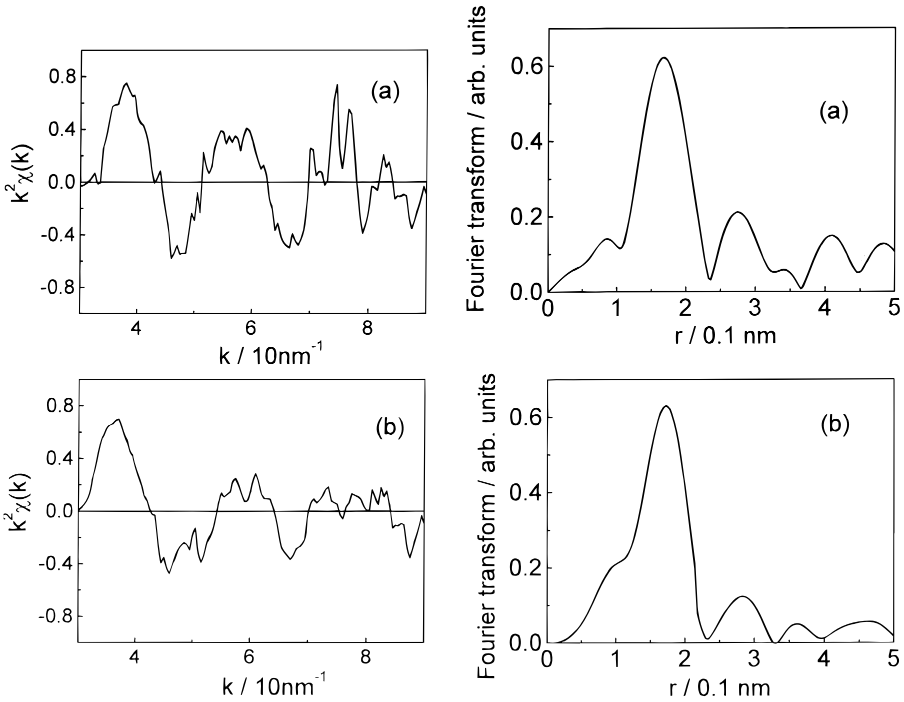

Figure 2. k^2-weighted EXAFS oscillations for species **A**: (a) p-polarization, (b) s-polarization. (B): Fourier transforms of the k^2-weighted EXAFS oscillations for species **A**, (a) p-polarization, (b) s-polarization.

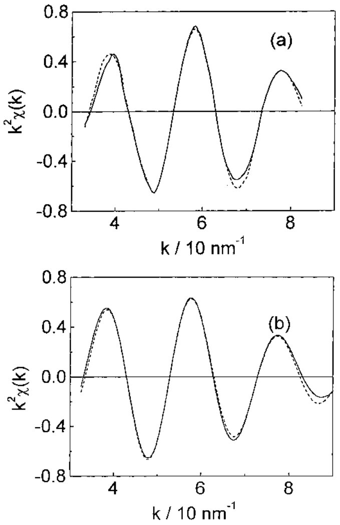

Figure 3. Best fitting results for inversely Fourier transformed data of the species **A**: (a) p-polarization; (b) s-polarization. Solid line, filtered data, broken line, calculated data.

TABLE 1: Curve-Fitting Results for Pt Species A on α-Al_2O_3(0001)

	Pt−O			
sample	N^*	r/nm	$\Delta\sigma^2$/nm	ΔE/eV
p-polarization	3.3 ± 0.5	0.198 ± 0.003	0.001 ± 0.001	3 ± 2
s-polarization	3.0 ± 0.5	0.201 ± 0.003	0.001 ± 0.001	3 ± 2

0.22 nm. Figure 3 shows the curve-fitting results in p-polarization and s-polarization. The structure parameters thus obtained are summarized in Table 1. The Pt−O bonds are found at about 0.200 ± 0.003 nm in both directions. The effective coordination numbers (N^*) for p-polarization and s-polarization are 3.3 and 3.0, respectively (Table 1). The effective coordination numbers were calculated using eq 8 assuming typical adsorption site models for Pt atoms on α-Al_2O_3(0001) in Table 2. We postulated three surface sites such as atop, bridge, and 3-fold sites on the unreconstructed α-Al_2O_3(0001) surface (O−O distance = 0.275 nm) as shown in Figure 4. Among the

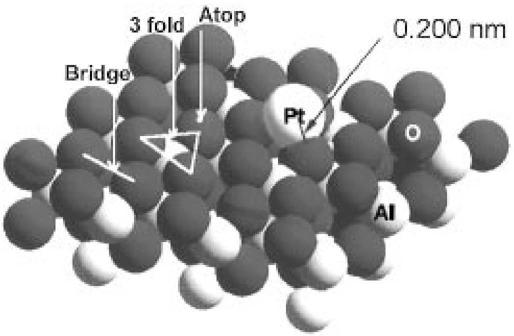

Figure 4. Model structure for species **A**.

TABLE 2: Calculated Effective Coordination Numbers (N^*) for Pt−O at Typical Three Adsorption Sites

	coordination number			
polarization	exptl	atop	bridge	3-fold
p	3.3 ± 0.5	1.6	2.4	3.1
s	3.0 ± 0.5	0.7	1.8	3.0

expected N^* values in both polarizations and their ratios for the three Pt sites, only the 3-fold site model can reproduce the observed data as shown in Table 2. The location of Pt atoms are illustrated in Figure 4. The α-Al_2O_3(0001) has two types of 3-fold hollow site which are distinguished by the presence of the underneath Al atom. Here the site which has no Al atom underneath the Pt is called as fcc site and the other site which has an Al atom below is called as hcp site. In our previous report Co atoms on α-Al_2O_3(0001) were demonstrated to occupy the fcc hollow sites of the surface where no Al was located under the Co atoms in the second surface layer of Al_2O_3 because we did not observe the Co−Al interaction in the p-polarization PTRF-EXAFS spectrum.[16] Although the peak appeared around 0.3 nm in Figure 2B, it was difficult to assign it to Pt−Al because the peak height is nearly in the noise level. In this work, we can not determine whether the location of Pt is fcc or hcp sites.

3.3. Structure of Pt Species B. Figure 5A shows the EXAFS oscillations for Pt species **B** prepared by the reduction

TABLE 3: Best Fitting Results of the EXAFS Data for Species B

	Pt−O				Pt−Pt			
	N	r/nm	$\Delta\sigma^2$/nm	ΔE/eV	N	r/nm	$\Delta\sigma^2$/nm	ΔE/eV
p-pol	1.5 ± 1.0	0.220 ± 0.009	0.003 ± 0.001	5 ± 2	3 ± 0.8	0.274 ± 0.003	0.001 ± 0.001	3 ± 2
s-pol	no[b]	no	no	no	6 ± 1	0.273 ± 0.003	0.002 ± 0.001	3 ± 2

[a] pol = polarization. [b] no = not observed.

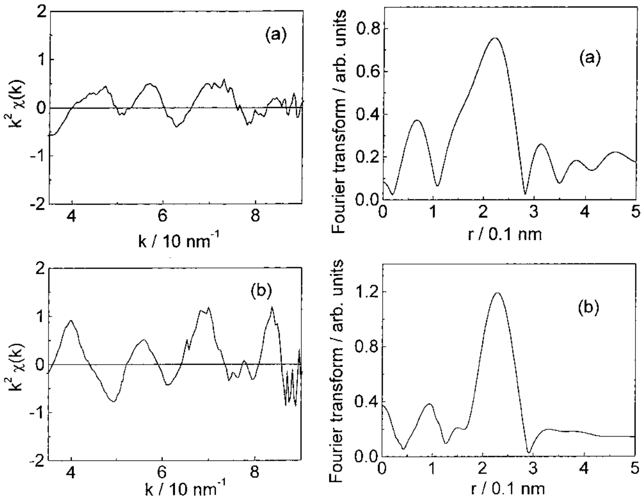

Figure 5. (A): k^2-weighted EXAFS oscillations of species **B** obtained by the reduction of species **A** with hydrogen at 373 K, (a) p-polarization, (b) s-polarization. (B): Fourier transforms of the k^2-weighted EXAFS oscillations for species **B**, (a) p-polarization, (b) s-polarization.

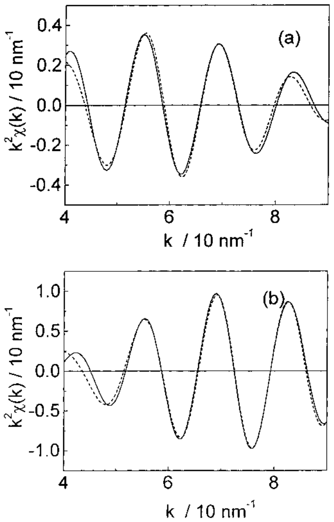

Figure 6. Best fitting results for the inversely Fourier transformed data of the species **B**: (a) p-polarization, (b) s-polarization. Solid line, observed data; broken line, calculated data.

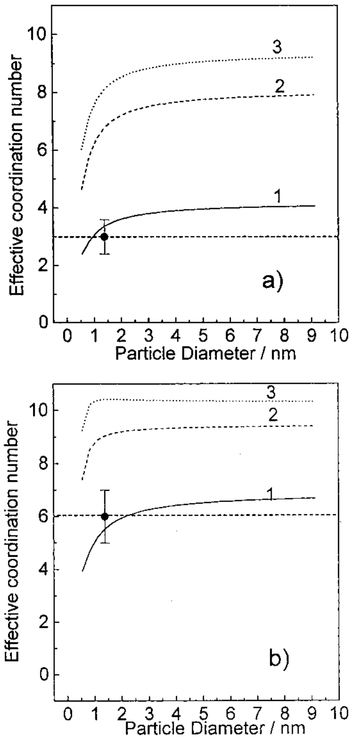

Figure 7. Calculated effective coordination numbers of Pt−Pt for s-polarization (a) and p-polarization (b) as a function of particle size based on the one-layer model (solid line 1), the two-layer model (broken line 2) and the three-layer model (dotted line 3). The observed data are given in a broken line with error bars.

of species **A** at 373 K with H_2 (Scheme 1). The oscillation in s-polarization lasts to the high k-region compared to that in p-polarization. Figure 5B shows the Fourier transformation of the EXAFS oscillations. The peak appears around 0.22 nm (phase shift: uncorrected) in both directions. However, the peak height for the Fourier transform of the p-polarization is 60% of that of the s-polarization. In addition, the p-polarization has a shoulder structure in the lower side of the main peak. We carried out a curve fitting analysis assuming that the main peak in s-polarization was due to Pt−Pt bonding. Since the shoulder structure appears only in p-polarization and it is attributable to Pt−O bonding, we carried out two-term fitting including Pt−Pt and Pt−O. Since the number of fitting parameters in the two-term fitting, 8, are near to the $N_{idp} = 9.6$ ($\Delta k = 60$ nm^{-1} and $\Delta r = 0.2$ nm), we fixed ΔE value to that obtained from EXAFS for s-polarization. Consequently, we obtained the best fitting depicted in Figure 6 and in Table 3. The larger error for Pt−O arises from the smaller contribution from the Pt−O than that from Pt−Pt and also the low signal to noise ratio of the observed data.

The Pt−Pt distances are determined to be 0.273 ± 0.003 nm, which is 0.005 nm shorter than that of Pt foil. The effective coordination number (N^*) of Pt−Pt for s-polarization is twice as large as that for p-polarization. If the Pt particles have a spherical shape, the N^* would give an equal value for s- and p-polarizations. Thus it is suggested that the anisotropic structures such as thin layer, semispherical, and ellipsoid are formed for Pt clusters on the Al_2O_3 surface. We calculated the N^* based on the models such as one atomic layer, two atomic layer, and three atomic layer raft using eq 8. Figure 7 shows the relation between N^* for Pt−Pt and the number of the layer as a function of the particle size (in diameter). The observed N^*'s, 3 for p-polarization and 6 for s-polarization, fit the expected values only for the one atomic layer raft structure. The other model, such as more than two layer, semisphere, and ellipsoid do not entirely reproduce the observed data. Furthermore, the particle size (diameter) of the Pt raft can be estimated to be ca 1.5 ± 0.5 nm from the observed and calculated N^* values for the p- and s-polarization as shown in Figure 7.

For the one layer raft structure a strong Pt-support interaction may be expected. In fact, we got the better fitting results for the p-polarization EXAFS when Pt−O was assumed. The Pt−O distance was determined as 0.220 ± 0.009 nm as shown in Table

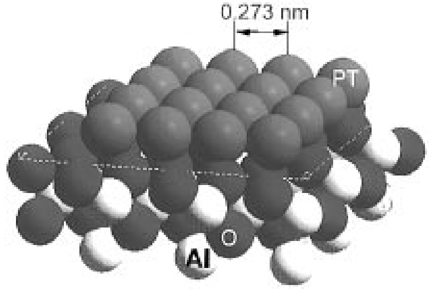

Figure 8. Model structure for species **B**.

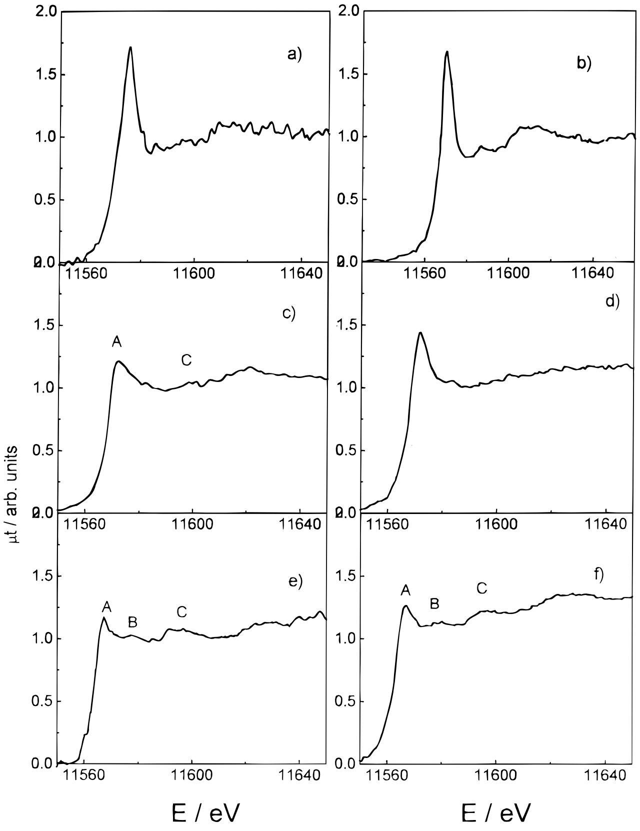

Figure 9. XANES spectra at Pt L_3-edge for species **A** (a, b), species **B** (c, d), and species **C** (e, f). Parts a, c, e are for s-polarization and parts b, d, f are for p-polarization.

3. The model structure for Pt rafts interacted with the oxygen layer of the α-Al_2O_3(0001) surface is illustrated in Figure 8.

3.4. Structure of Pt Species Reduced after 673 K. When the Pt clusters were reduced at 673 K, the Pt atoms were aggregated to 3-dimensional particles. Figure 9 shows the polarization-dependent XANES spectra at the L_3 edge of Pt species on α-Al_2O_3(0001). The L_3-edge peak intensity reflects the vacancy of the 5 d state,[30-32] i.e., stronger white line peak suggests more electron deficiency in d state. The species **A** exhibits a strong edge peak for both s- and p-polarizations, which indicates that the Pt atoms possess positive charge induced by the Pt−O−Al bonding as shown in Figure 4.

The species **B** formed by the reduction at 373 K shows different XANES spectra between s- and p-polarizations. The XANES feature of species **B** for s-polarization (Figure 9c) is similar to that of the supported small Pt metal particles adsorbed by hydrogen, the feature of which was characterized by the broadening of the white line peak to the higher energy with decreasing the edge height induced by the adsorption of hydrogen.[30,33-40] On the other hand, the XANES spectrum in p-polarization shows a strong white line peak[30,31] indicating the presence of the more vacancy in the d electron states perpendicular to the surface which is caused by the Pt−O bonding as was detected in EXAFS. On the other hand, The XANES spectrum is s-polarization (Figure 9c) resembles the metallic Pt particles reflecting metal−metal bonding. Thus these facts also support the raftlike structure of Pt particles strongly interacted with surface oxygen well corresponding to the EXAFS results described in section 3.3.

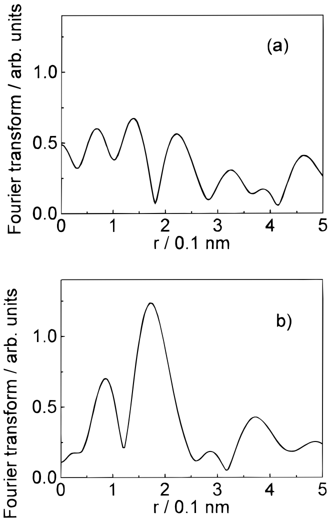

Figure 10. (b) Fourier transforms of the k^2-weighted EXAFS oscillations for species **D** after the reaction of species **B** with NO: (a) p-polarization, (b) s-polarization.

After the reduction of the species **B** at 673 K, the XANES spectra for s- and p-polarizations were found to be similar to each other (Figure 9e,f). The structures A, B, and C in the XANES spectra of Figures 9e,f appeared at the same positions as those for Pt foil, which suggests the formation of Pt particles. No polarization dependence of the XANES spectra indicates the growth of three-dimensional Pt particles on the α-Al_2O_3-(0001) surface after the 673 K reduction.

3.5. Structure of Species D after the Exposure of B to NO. When species **B** was exposed to NO at room temperature, the Pt−Pt bond was cleaved. As shown in Figure 10b, no peak due to Pt−Pt bond appeared in the Fourier transform for s-polarization in which the Pt−Pt peak in the sample B had been observed before NO adsorption. The Pt raft was destroyed to monomer species by the interaction with NO. The peak observed in the Fourier transform (Figure 10b) was analyzed to be due to Pt−O at 0.205 nm. In the p-polarization spectrum, we were not able to find definite EXAFS oscillation and no peak above noise level was observed in Figure 10a. The EXAFS oscillation for p polarization might be composed of platinum−oxygen (support) and Pt−NO (adsorbed). We infer that the EXAFS oscillation might smear out because of the interference of the different interatomic distances between platinum−oxygen (support) and platinum-adsorbates. Pt−Pt bond was cleaved in the *species* **D** after the exposure to NO and Pt monomer adsorbed with NO was created on the Al_2O_3 surface though the further study is necessary to draw the definite structure for the *species* **D**.

4. Discussion

4.1. Structure of Species A and Its Catalytic Activities. The Pt/α-Al_2O_3 and the Pt/SiO_2 catalysts derived from $Pt_4(\mu\text{-}CH_3COO)_8$ as precursor show high activity for the selective dehydrogenation of HCOOH described above. While the Pt/SiO_2 has a long induction period, the Pt/α-Al_2O_3 shows no induction period (Figure 1). The active species on Pt/SiO_2 was found to be Pt monomers which were bound to the SiO_2 surface

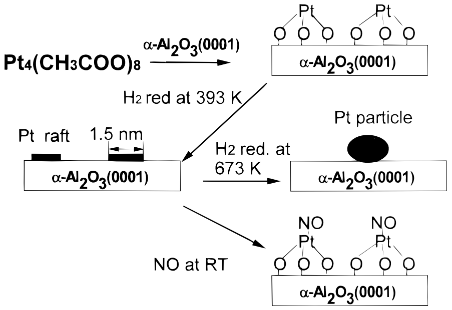

Figure 11. Structural transformation of the Pt species on α-Al_2O_3(0001).

making Pt−O bonds.[29] During the induction period the $Pt_4(\mu\text{-}CH_3COO)_8$ cluster framework on SiO_2 was decomposed to monomers via a Pt dimer structure with the Pt−Pt distance at 0.250 nm by the exposure to HCOOH. The present EXAFS analysis reveals that Pt monomers are readily formed with 0.200 ± 0.003 nm on 3-fold site of α-Al_2O_3(0001) surface after the deposition of $Pt_4(\mu\text{-}CH_3COO)_8$ cluster. Since the Pt monomer structure has already been present before the catalytic reaction, there is no induction period in the reaction. Such a different behavior of $Pt_4(\mu\text{-}CH_3COO)_8$ clusters on SiO_2 and Al_2O_3 can be compared to the different structural transformation of Ru clusters and Rh dimers on SiO_2 and Al_2O_3,[40,41] where the metal−metal bonds of the cluster and the dimer were observed on SiO_2 surface though the atomically dispersed species were present on the Al_2O_3.

4.2. Raftlike Structure of the Species B. Raftlike structures of supported metal particles have been proposed for Ru/SiO_2, Os/SiO_2, Ru-Os/SiO_2, and Ir-Pt/Al_2O_3 by transmission electron microscopy (TEM) and EXAFS and Ru−Cu particles on SiO_2 by TEM and EXAFS.[1,42−45] Yates et al. also reported a raft structure for Rh particles on Al_2O_3 by means of TEM, chemisorption, and IR.[46] The raftlike structures have also been demonstrated by observing the direct metal−oxygen(support) bonding.[47−51] The PTRF-EXAFS can determine more directly the raft structure by comparing the EXAFS oscillations in two directions, perpendicular, and parallel to the surface. The PTRF-EXAFS showed the presence of metal−oxygen (support) bond which was difficult to detect by conventional EXAFS because a small contribution of the metal−oxygen bonding as compared to a large contribution of the metal−metal bonding except for very small metal cluster systems. Koningsberger et al. used a difference file method to remove the large contribution of metal−metal bonding.[51] They reported the metal−oxygen distances in the supported noble metal powder catalysts which were present around 0.25−0.27 nm when the sample was reduced at low temperatures and in the presence of H_2, while the Pt−O bond length decreased to ca. 0.22 nm when the sample was evacuated or reduced at high temperatures (>723 K).[52] In the present work on the α-Al_2O_3(0001) single-crystal surface we found the Pt−O distance at 0.220 nm even reduced with H_2 at low temperature (373 K) and in the presence of H_2 which indicated the formation of the covalent bonds between Pt atoms and surface oxygen atoms. Such a strong Pt−O interaction stabilizes the Pt raftlike structure.

5. Conclusions

In this paper, we have reported the polarization-dependent total-reflection fluorescence XAFS (EXAFS and XANES) studies on the Pt cluster on α-Al_2O_3(0001). This technique gives clearer information on adsorption sites of metal atoms, metal−support, and metal−metal bondings, and anisotropic surface structures. The structural transformation of the Pt_4 clusters on α-Al_2O_3(0001) is summarized in Figure 11. The Pt_4 cluster framework is destroyed to Pt monomers which occupy the 3-fold hollow sites of the oxygen atoms of α-Al_2O_3(0001) surface, making Pt−O bonds at the distance of 0.200 ± 0.003 nm. The isolated Pt atoms are reduced to one-atomic layer thick raft cluster with H_2 at 373 K. The Pt−Pt and Pt−O bondings are observed at 0.273 nm and 0.220 nm, respectively. The Pt rafts are redispersed to Pt monomers by the exposure of NO, or agglomerated to three-dimensional particles by the 673 K reduction.

Acknowledgment. The authors would like to express thanks to Prof. M. Nomura in PF and Dr. T. Yokoyama in the Unversity of Tokyo for their kind technical supports. The work was carried out under the approval of PF advisory committee (Proposals 90142, 92G174). This work has been supported by CREST (Core Research for Evolutional Science and Technology) of Japan Science and Technology Corporation (JST).

References and Notes

(1) Greegor, R. B.; Lytle, F. W. *J. Catal.* **1980**, *63*, 476.

(2) Koningsberger, D. C.; Prins, R. *X-ray Absorption, Principles, Applications, Techniques of EXAFS, SEXAFS, and XANES*; John Wiley & Sons: New York, 1988; Vol. 92.

(3) Iwasawa, Y. *X-ray Absorption Fine Structure for Catalysts and Surfaces*; World Scientific: Singapore, 1996; Vol. 2.

(4) Stohr, J.; Kollin, E. B.; Fischer, D. A.; Hastings, J. B.; Zaera, F.; Sette, F. *Phys. Rev. Lett.* **1985**, *55*, 1468.

(5) Fischer, D. A.; Hastings, J. B.; Zaera, F.; Stohr, J.; Sette, F. *Nucl. Instrum. Methods Phys. Res.* **1986**, *A246*, 561.

(6) Funabashi, M.; Ohta, T.; Yokoyama, T.; Kitajima, Y.; Kuroda, H. *Rev. Sci. Instrum.* **1989**, *60*, 2505.

(7) Funabashi, M.; Yokoyama, T.; Takata, Y.; Ohta, T.; Kuroda, H. *Surf. Sci.* **1990**, *242*, 59.

(8) Stohr, J. *X-ray Absorption Principles, Applications, Techniques of EXAFS, SEXAFS, and XANES*; Prins, R., Koningsberger, D. C., Eds.; A John Wiley & Sons: New York, 1988; p 443.

(9) Ohta, T. *X-ray Absorption Fine Structure for Catalysts and Surfaces*; Y. Iwasawa, Ed.; World Scientific: Singapore, 1996; Vol. 2, p 354.

(10) Parratt, L. G. *Phys. Rev.* **1954**, *95*, 359.

(11) Heald, M.; Keller, E.; Stern, E. A. *Phys. Lett.* **1984**, *103A*, 155.

(12) Shirai, M.; Iwasawa, Y. *XAFS Application to Catalysis and Surface*; Y. Iwasawa, Ed.; Elsevier: Amsterdam, 1996; p 332.

(13) Shirai, M.; Asakura, K.; Iwasawa, Y. *Catal. Lett.* **1992**, *15*, 247.

(14) Shirai, M.; Asakura, K.; Iwasawa, Y. *Catal. Lett.* **1992**, 1037.

(15) Shirai, M.; Asakura, K.; Iwasawa, Y. *Jpn. J. Appl. Phys., Part 1* **1993**, *32−2*, 413.

(16) Shirai, M.; Inoue, T.; Onishi, H.; Asakura, K.; Iwasawa, Y. *J. Catal.* **1994**, *145*, 159.

(17) Shirai, M.; Asakura, K.; Iwasawa, Y. *Catal. Lett.* **1994**, *26*, 229.

(18) Shirai, M.; Nomura, M.; Asakura, K.; Iwasawa, Y. *Rev. Sci. Instrum.* **1995**, *66*, 5493.

(19) Yamaguchi, T.; Sasaki, Y.; Nagasawa, A.; Ito, T.; Koga, N.; Morokuma, K. *Inorg. Chem.* **1989**, *28*, 4311.

(20) Yamaguchi, T. Doctoral Thesis, Tohoku University, 1989.

(21) Yamaguchi, T.; Sasaki, Y.; Ito, T. *J. Am. Chem. Soc.* **1990**, *112*, 4038.

(22) Nomura, M.; Koyama, A.; Sakurai, M. *KEK Report* **1991**, *91−1*, 1.

(23) Asakura, K. *X-ray Absorption Fine Structure for Catalysts and Surfaces*; Iwasawa, Y., Ed.; World Scientific: Singapore, 1996; Vol. 2; p 33.

(24) Rehr, J. J.; Mustre de Leon, J.; Zabinsky, S. I.; Albers, R. C. *J. Am. Chem. Soc.* **1991**, *113*, 5135.

(25) Lytle, F. W. Sayers, D. E.; Sterns, E. A. *Physica B* **1988**, *158*, 701. Report on the International Workshops on Standards and Criteria in XAFS, York. Proceedings *XAFS 6* **1990**, 751.

(26) Stern, E. *Phys. Rev. B* **1993**, *48*, 9825.

(27) Teo, B. K.; Lee, P. A. *J. Am. Chem. Soc.* **1979**, *101*, 2815.

(28) Comin, F.; Citrin, P. H.; Eisenberger, P.; Rowe, J. E. *Phys. Rev. B* **1982**, *26*, 7060.

(29) Chun, W. J.; Tomishige, K.; Hamakado, M.; Iwasawa, Y.; Asakura, K. *J. CChem. Soc., Faraday Trans.* **1995**, *91*, 4161.

(30) Lytle, F. W.; Wei, P. S. P.; Greegor, R. B.; Via, G. H.; Sinfelt, J. H. *J. Chem. Phys.* **1979**, *70*, 4849.

(31) Horsley, J. A. *J. Chem. Phys.* **1982**, *76*, 1451.

(32) Mansour, A. N.; Cook, J. W.; Sayers, D. E. *J. Phys. Chem.* **1984**, *88*, 2330.

(33) Samant, M. G.; Boudart, M. *J. Phys. Chem.* **1991**, *95*, 4070.

(34) McHugh, B. J.; Larsen, G.; Haller, G. L. *J. Phys. Chem.* **1990**, *94*, 8621.

(35) Vaarkamp, M.; Miller, J. T.; Modica, F. S.; Lane, G. S.; Koningsberger, D. C. *Proc. Int. Cong. Catal.* **1992**, *10*, 809.

(36) Vaarkamp, M.; Modica, F. S.; Miller, J. T.; Koningsberger, D. C. *J. Catal.* **1993**, *144*, 6111.

(37) Vaarkamp, M.; Miller, J. T.; Modica, F. S.; Koningsberger, D. C. *Jpn. J. Appl. Phys.* **1993**, *32*−*2*, 454.

(38) Ichikuni, N.; Iwasawa, Y. *Catal. Lett.* **1993**, *20*, 87.

(39) Kubota, T.; Asakura, K.; Ichikuni, N.; Iwasawa, Y. *Chem. Phys. Lett.* **1996**, *256*, 445.

(40) (a) Asackura, K.; Kubota, T.; Ichikuni, N.; Iwasawa, Y. In *Proceedings of the 11th International Congress on Catalysts*; Elsevier Science B.V.: Baltimore, MD, 1996; p 911. (b) Asakura, K.; Iwasawa, Y. *J. Chem. Soc., Faraday Trans. 1* **1988**, *84*, 2445.

(41) Bando, K. K.; Asakura, K.; Arakawa, H.; Isobe, K.; Iwasawa, Y. *J. Phys. Chem.* **1996**, *100*, 13636.

(42) Prestridge, E. B.; Via, G. H.; Sinfelt, J. H. *J. Catal.* **1977**, *50*, 115.

(43) Lytle, F. W.; Via, G. H.; Sinfelt, J. H. *J. Chem. Phys.* **1977**, *67*, 3831.

(44) Via, G. H.; Sinfelt, J. H.; Lytle, F. W. *J. Chem. Phys.* **1979**, *71*, 690.

(45) Sinfelt, J. H.; Via, G. H.; Lytle, F. W. *J. Chem. Phys.* **1982**, *76*, 2779.

(46) Yates, D. J. C.; Murrel, L. L.; Prestridge, E. B. *J. Catal.* **1979**, *57*, 41.

(47) Fung, A. S.; Tooley, P. A.; Kelly, M. J.; Koningsberger, D. C.; Gates, B. C. *J. Phys. Chem.* **1991**, *95*, 225.

(48) Van Zon, F. B. M.; Maloney, S. D.; Gates, B. C.; Koningsberger, D. C. *J. Am. Chem. Soc.* **1993**, *115*, 10317.

(49) Asakura, K.; Yamada, M.; Iwasawa, Y.; Kuroda, H. *Chem. Lett.* **1985**, 511.

(50) Asakura, K.; Iwasawa, Y. *J. Chem. Soc., Faraday Trans.* **1990**, *86*, 2657.

(51) van Zon, J. B. A. D.; Koningsberger, D. C.; van’t Blik, H. F. J.; Prins, R.; Sayers, D. E. *J. Chem. Phys.* **1984**, *80*, 3914.

(52) Koningsberger, D. C.; Gates, B. C. *Catal. Lett.* **1992**, *14*, 271.